coatings

MDPI

Article

Calculation and Lubrication Characteristics of Cylindrical Roller Bearing Oil Film with Consideration of Thermal Effects

Mian Zhang [1], Xiqiang Ma [1,2,3,*], Nan Guo [1,3], Yujun Xue [1,2,3] and Jishun Li [1,3]

[1] School of Mechatronics Engineering, Henan University of Science and Technology, Luoyang 471003, China
[2] Longmen Laboratory, Luoyang 471003, China
[3] Henan Key Laboratory for Machinery Design and Transmission System, Henan University of Science and Technology, Luoyang 471003, China
* Correspondence: maxiqiang@haust.edu.cn

Abstract: Aiming at the problem of how the thermal characteristics of cylindrical roller bearings affect the lubrication characteristics of bearings under actual working conditions, the influence of parameters such as speed and load on the lubrication characteristics of cylindrical roller bearings under thermal effects is analyzed. The numerical calculation method combining the quasi-static model of cylindrical roller bearing and the thermal elastohydrodynamic lubrication model is adopted. The effects of rotational speed, load and thermal effect on the lubrication performance of the bearing and the lubrication state under certain oil supply conditions were analyzed via numerical model calculation. The oil film thickness was measured via an immersion ultrasonic method to verify the correctness of the model. The results show that the larger the bearing speed, the larger the central film thickness and the minimum film thickness. At the same time, the thermal effect on the film thickness is more obvious; the greater the load, the greater the maximum oil film pressure. The film thickness gradient in the inlet region is greatly reduced, but the thermal effect has no obvious effect on the overall film thickness. In addition, there is a critical value of effective lubrication film thickness for each set of operating parameters. When the actual film thickness is equal to the critical value, the bearing lubrication state is at its best; the numerical simulation results are compared with the experimental values. Under the calculation conditions, the maximum error at the measuring point is within 10%, which meets the error requirements and provides a theoretical basis for revealing the bearing lubrication mechanism.

Keywords: cylindrical roller bearing; line contact; thermal elastohydrodynamic lubrication; lubrication properties; thermal effect

check for updates

Citation: Zhang, M.; Ma, X.; Guo, N.; Xue, Y.; Li, J. Calculation and Lubrication Characteristics of Cylindrical Roller Bearing Oil Film with Consideration of Thermal Effects. *Coatings* **2023**, *13*, 56. https://doi.org/10.3390/coatings13010056

Academic Editors: Miroslav Kohl and Diego Martinez-Martinez

Received: 11 November 2022
Revised: 15 December 2022
Accepted: 23 December 2022
Published: 28 December 2022

Copyright: © 2022 by the authors. Licensee MDPI, Basel, Switzerland. This article is an open access article distributed under the terms and conditions of the Creative Commons Attribution (CC BY) license (https://creativecommons.org/licenses/by/4.0/).

1. Introduction

Cylindrical roller bearing and raceway between line contact have the advantages of small friction torque, low friction loss, convenient lubrication, and maintenance, and they are widely used in aero-engine operation systems [1,2]. Relevant data show that the contact area lubrication failure is caused by the bearing and is the main reason for wear and failure. A good lubrication state is maintained as an effective measure to reduce wear and avoid failure of rolling bearings [3–9]. In the lubrication process, the oil film is heated by viscous shear and compression, resulting in an increase in temperature, causing the oil film thickness and pressure to change. The physical and chemical properties of the lubricant are often changed by the temperature rise of the contact area. In more serious cases, this will lead to rupture and failure of the lubricating film, and producing different degrees of adhesive wear on the contact surface. It can even lead to sticking issues. Therefore, it is necessary to analyze the lubrication characteristics of the bearing contact area under thermal effect. It provides a reference for applications for improving the reliability of aero-engine operation systems.

Many foreign and native scholars have conducted a lot of research on the lubrication characteristics of the contact area of cylindrical roller bearings. Qiu et al. [10–13] calculated the dynamic characteristics of the cylindrical roller bearing contact micro-zone, calculated the oil film thickness and analyzed the bearing lubrication characteristics by using the quasi-static method and the elastohydrodynamic lubrication (EHL) model. The thermal effect, non-Newtonian and other factors were considered based on the Dowson empirical formula by Marian et.al [14]. The empirical formula reduces the calculation accuracy, although it simplifies the calculation. High reliability is required, and large calculation errors could lead to immeasurable losses, especially for high-precision bearings. Chen et al. [15] used the multi-grid technique to numerically simulate the line contact thermal EHL. It not only improved the iterative speed of calculation, but also enhanced the calculation accuracy to some extent. Considering the influence of thermal effect on the lubrication characteristics of thermoelastic fluid in line contact, Zhao et al. [16,17] established a thermoelastic fluid model, analyzed the change trend of oil film pressure and oil film thickness and studied the influence of thermal effect on the lubrication ability of the contact interface under harsh working conditions. Bai et al. [18] established a EHL model and studied the influence of different oil-supply conditions on the lubrication characteristics of bearings.

The traditional methods for measuring the thickness of lubricating oil film include optical interference, the resistance method and so on. However, due to the limitations of these methods, they cannot be applied to the measurement of bearing film thickness under real working conditions. Ultrasonic has the characteristics of high frequency, strong penetration ability and good directivity. This ultrasonic nondestructive testing technology has become an important research method for domestic and foreign researchers to carry out bearing film thickness measurement. Duan et al. [19] measured the film thickness of cylindrical roller bearings using the ultrasonic method, and the minimum film thickness of bearings under different loads and speeds was analyzed. The relative error between theoretical calculation and experimental results was small. The test verified the accuracy of the theoretical results. Li Meng et al. [20] proposed an ultrasonic measurement method under mixed lubrication and established a parallel model of the interface oil film stiffness and the contact stiffness of the rough body. By introducing the contact coefficient and combining the empirical formula to decompose the total interface stiffness measured by the ultrasonic method, the oil film stiffness under mixed lubrication was obtained, and then a more accurate oil film thickness was obtained. Beamish et al. [21] introduced a new method for measuring oil film thickness based on a spring model. The advantage of this method over existing techniques is that it can be applied to thin, multilayer materials to measure oil film thickness more accurately.

At present, due to the practical application of rolling bearings in harsh working conditions, the calculation of lubricating oil film thickness is mostly carried out in an ideal state. In this paper, the quasi-static model and heat flow field model of cylindrical roller bearing are established according to the actual working conditions. The influencing factors of bearing lubrication performance are analyzed, and the change rule of bearing lubrication performance considering thermal effect is revealed. The relationship between effective lubricating film thickness and the initial position of the oil film in the bearing contact area is discussed. Finally, an ultrasonic monitoring test bench is built to realize the monitoring and analysis of the cylindrical roller bearing, which verifies the correctness of the theoretical calculation results and has certain engineering application value. It provides an application reference for improving the lubrication performance of cylindrical roller bearings.

2. Theoretical Method

The mathematical model of steady-state line contact thermal EHL consists of the Reynolds equation, film thickness equation, load balance equation, energy equation, thermal boundary equation, motion equation, and two empirical formulas of viscosity–temperature pressure and density–temperature pressure.

This is shown in Equation (1):

$$\frac{d}{dx}\left(\frac{\rho h^3}{\eta}\frac{dp}{dx}\right) = 12u_r\frac{d(\rho h)}{dx} \tag{1}$$

In the formula, η is the initial viscosity of the lubricant; u_r is the average speed of the bearing surface; ρ is the lubricant density.

The boundary conditions are:

Entrance:

$$p(x_{in}) = 0 \tag{2}$$

Export:

$$\frac{\partial p(x_{out})}{\partial x} = 0,\ p(x_{out}) = 0 \tag{3}$$

The film thickness equation is:

$$h(x) = h_0 + \frac{x^2}{2R} + \delta(x) \tag{4}$$

In the formula:

$$\delta(x) = -\left(\frac{2}{\pi E'}\int_{s_2}^{s_1} p(s)\ln(s-x)^2 ds + c\right) \tag{5}$$

In the formula, $E^{'}$ is the equivalent total elastic modulus; h_0 is the initial film thickness; R is the equivalent radius of curvature, and $\delta(x)$ is the elastic deformation of the roller at any given point under pressure.

The energy equation is:

$$cpu\frac{\partial T}{\partial x} = k\frac{\partial^2 T}{\partial z^2} - \frac{T}{\rho}\frac{\partial \rho}{\partial T}u\frac{\partial p}{\partial x} + \eta\left(\frac{\partial u}{\partial z}\right)^2 \tag{6}$$

In the formula, c represents the specific heat capacity of the lubricant, k is the heat conduction system, and T is the boundary surface temperature.

The empirical formula of viscosity–pressure–temperature is [22,23]:

$$\eta = \exp\left\{(\ln\eta_0 + 9.67)\left(1 + 5.1\times10^{-9}p\right)^{Z'}\left(\frac{T-138}{T_0-138}\right)^{-s_0} - 1\right\} \tag{7}$$

In the formula, the constant z' can be determined by the viscosity–pressure coefficient in the Barus exponential relationship in the absence of experimental data. T_0 is the ambient temperature and η_0 is the initial viscosity.

The empirical formula of density–pressure–temperature is [22,23]:

$$\rho = \rho_0\left[1 + \frac{0.6p}{1+1.7p} + D(T-T_0)\right] \tag{8}$$

In this equation, p the film pressure ρ_0 is the initial density and D is the constant.

The load balance equation is:

$$\int_{x_{in}}^{x_{out}} p(x)dx = w \tag{9}$$

In the formula, w is the unit load; the unit is N/m.

The thermal boundary equation is:

$$T_1(0,x) = \frac{kR_x}{\sqrt{\pi\rho_1 c_1 k_1 u_1 b^3}}\int_{-\infty}^{x}\frac{\partial T}{\partial z}\frac{ds}{\sqrt{x-s}} + T_0 \tag{10}$$

$$T_2(0,x) = \frac{kR_x}{\sqrt{\pi\rho_2 c_2 k_2 u_2 b^3}}\int_{-\infty}^{x}\frac{\partial T}{\partial z}\frac{ds}{\sqrt{x-s}} + T_0 \tag{11}$$

In the formula, k_1 and k_2 are the heat conductions coefficient of the inner and outer bearing rings; ρ_1 and ρ_2 is the density of the inner and outer bearing rings; c_1 and c_2 is the specific heat capacity for the inner and outer ring bearing; u_1 and u_2 linear velocity at the contact point for the inner and outer rings of the bearing.

The equation of motion is:

$$\frac{\partial u}{\partial z} = \frac{\partial p}{\partial x}\frac{1}{\eta}(z - z_m) + \frac{1}{\eta}\frac{u_2 - u_1}{FU_0} \tag{12}$$

$$u = u_1 + \frac{u_2 - u_1}{FU_0}\int_0^z \frac{dz}{\eta} + \frac{\partial P}{\partial X}\left(\int_0^z \frac{z}{\eta}dz - z_m\int_0^Z \frac{dz}{\eta}\right) \tag{13}$$

In the formula:

$$\overline{FU_0} = \int_0^h \frac{1}{\overline{\eta}}dz \tag{14}$$

$$\overline{FU_1} = \int_0^h \frac{z}{\overline{\eta}}dz \tag{15}$$

$$z_m = \frac{\overline{FU_1}}{\overline{FU_0}} \tag{16}$$

3. Numerical Analysis Method

Numerical analysis is carried out in a post-dimensionless state. It is defined as non-deterministic stack automaton-dimensional coordinates $X_{out} = x_{out}/b$, $X_{in} = x_{in}/b$, $X = x/b$; non-dimensional pressure $P = p/p_H$, $\overline{\eta} = \eta/\eta_0$, $\overline{\rho} = \rho/\rho_0$, $P_H = E^{'}b/4R$; dimensionless film thickness $H = h/h_0$; dimensionless load $W = w/\left(E^{'}R\right)$; non-dimensional velocity $U = u_r\eta_0/E^{'}R$, $u_r = (u_1 + u_2)/2$. The pH is the maximum Hertz contact pressure, and b is the Hertz contact half-width.

Taking the cylindrical roller bearing as an example, the situation is analyzed where the entrainment velocity under full-film lubrication is consistent with the direction X (the dimensionless coordinate along the direction of roller motion). It is assumed that the Newtonian fluid is compressible, and the calculation process of oil film pressure and film thickness distribution is shown in Figure 1.

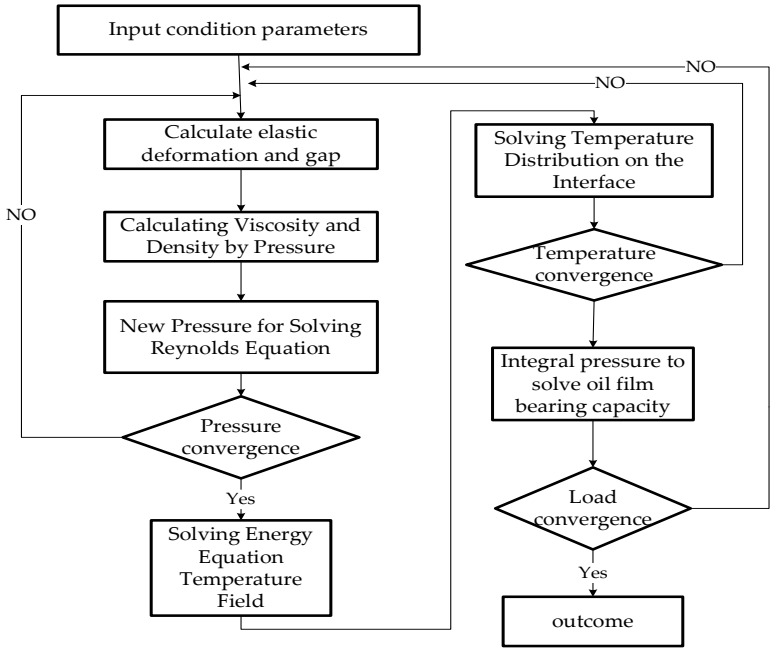


Figure 1. Thermal EHL numerical analysis process.

Firstly, given the structural, lubricant, and working-condition parameters of the bearing, a quasi-static model of a cylindrical roller bearing is established [24,25]. The Newton–Raphson method is used to solve the model, and the micro-zone motion and force state between the rolling element as well as the inner and outer raceways are obtained. Later, the working condition of the contact area is brought into the thermal EHL calculation model. The numerical solution is obtained using a multigrid method. The densest grid layer has 129 equidistant nodes. When the relative errors of pressure and load are less than 1×10^{-4}, the pressure and the final numerical solution are obtained via iteration.

4. Results and Discussion

The main parameters and working parameters of cylindrical roller bearings are shown in Tables 1 and 2. Lubricating oil 4109 was selected. Its viscosity at room temperature was 0.033 Pa·s, the viscosity–pressure coefficient was 1.28×10^{-8} Pa^{-1}, the viscosity-temperature coefficient was 0.032 $^{\circ}C^{-1}$ and the thermal conductivity was 0.0966 $N/(s.^{\circ}C)$.

Table 1. Main parameters of cylindrical roller bearings.

Major Parameter	Numerical Value
Bearing bore diameter/(mm)	110
Bearing outside diameter/(mm)	156
Roller diameter/(mm)	11
Roller contact length/(mm)	11
Roller number	30
Elastic modulus of inner and outer ring/(GPa)	208
Elastic modulus of rolling element/(GPa)	308
Poisson's ratio of inner and outer ring	0.3
Rolling body Poisson's ratio	0.26
Inner and outer ring density/(kg/m^3)	7840
Roller density/(kg/m^3)	3200

Table 2. Operating parameters of cylindrical roller bearings.

Working Condition	Radial Load (kN)	Rotate Speed (r/min)
1	3	2000
2	8	2000
2	12	2000
4	12	2500
5	12	500

Research on the lubrication reliability of cylindrical roller bearings generally analyzes the most heavily loaded areas of the bearing [26]. In this paper, the contact area parameters between the outer ring raceway and roller are selected to establish the thermal EHL model and analysis bearing lubrication characteristics. During service, the bearing inevitably has a start–stop stage and runs at a lower speed, and in engineering practice, especially at low speeds, direct contact is usually the main cause of bearing failure [27–29]. Therefore, this paper includes five kinds of working condition parameters in Table 2 as examples. The contact load of the maximum loaded roller, and the corresponding entrainment speed under different working conditions, are obtained by establishing the quasi-static model of cylindrical roller bearing, using the Newton–Raphson method to calculate the working conditions shown in Table 2. Table 3 shows the results of the quasi-static calculation. It can be seen from Table 3 that the contact load between the rolling element with the largest load and the inner and outer rings is not very different. The results of quasi-static calculation are shown in Table 3.

Table 3. Results of pseudo-statics calculation.

Working Condition	Maximum Contact Load Between Rolling Element and Inner Ring (N/m)	Maximum Contact Load Between Rolling Element and Outer Ring (N/m)	Entrainment Velocity (m/s)
1	1.23×10^5	1.24×10^5	6.9
2	2.54×10^5	2.55×10^5	6.9
3	3.46×10^5	3.47×10^5	6.9
4	3.46×10^5	3.47×10^5	8.6
5	3.46×10^5	3.47×10^5	1.7

4.1. Analysis of Influence Factors of Line Contact Thermal EHL

4.1.1. Influence Analysis of Load Parameters

Conditions 1, 2 and 3 show the cylindrical roller bearing roller, outer ring maximum load rolling element and movement direction of oil film pressure and film thickness distribution. As the radial load parameters increases, the maximum oil film pressure gradually increases, and the secondary pressure peak gradually moves to the outlet area, as shown in Figure 2. The film thickness gradient in the inlet area is greatly reduced, and the necking phenomenon becomes more evident and gradually moves to the contact center, but the center film thickness remains almost unchanged.

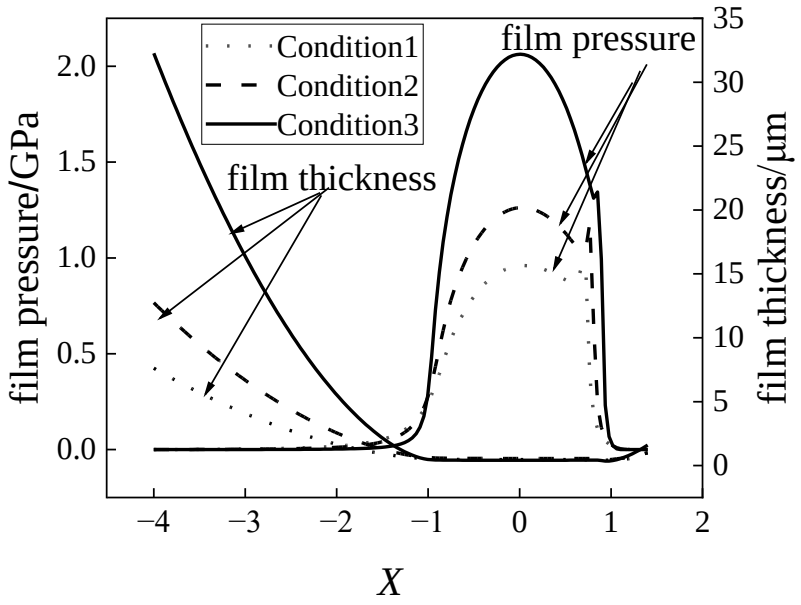


Figure 2. Effect of radial load on thermal EHL.

Under conditions 1 and 3, through the numerical calculation of isothermal EHL and thermal EHL, the influence of load parameters on the film thickness distribution is shown in Figure 3. From the isothermal solution and the changing trend of pyrolysis film thickness under working conditions 1 and 3 in Figure 3, it can be seen that the thermal effect does not change the film thickness as a whole. However, the minimum oil film thickness gradually decreases, and the oil film necking converges to the inlet area. The main reason is that the increase in temperature is not conducive to the formation of an oil film.

Figure 4 shows the influence trend of load parameters on oil film pressure through the numerical calculation of Isothermal EHL and thermal EHL under working conditions 1 and 3. The Hertz contact pressure is about 1.2 and 2.1 GPa under conditions 1 and 3 in Figure 4. The changing trend of isothermal solution and pyrolysis oil film pressure under this working condition is analyzed. It can be seen that the thermal effect has little impact on the oil film pressure. Considering the thermal effect, the secondary pressure peak of the oil film is closer to the inlet direction.

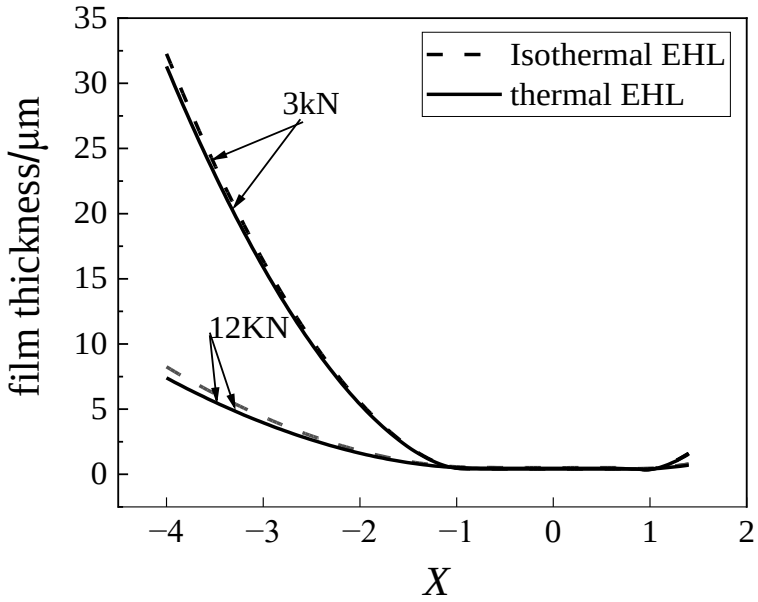


Figure 3. Effect of radial load on film thickness distribution.

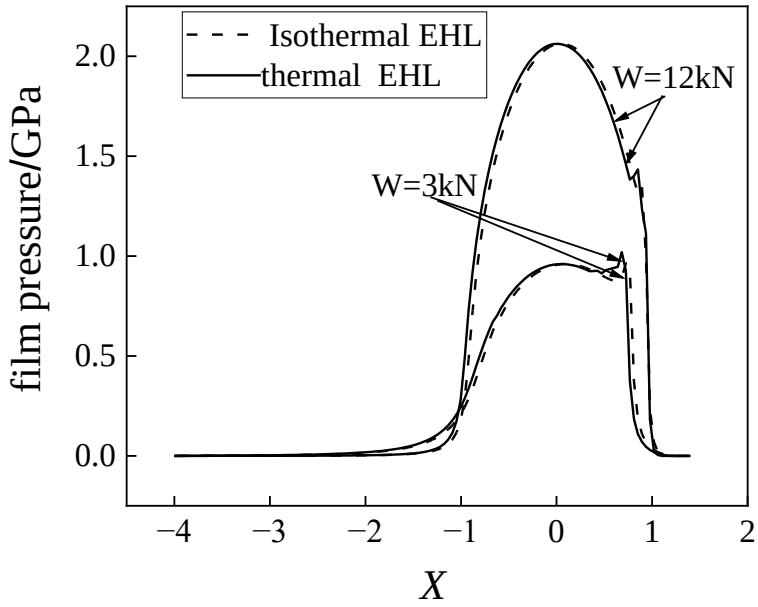


Figure 4. Effect of Radial Load on Oil Film Pressure Distribution.

4.1.2. Influence Analysis of Velocity Parameters

Figure 5 shows the distribution of oil film pressure and film thickness in the *X* direction of the roller consisting of the largest load on the outer ring of the cylindrical roller bearing under working conditions 3, 4 and 5. From Figure 5, it can be seen from the oil film distribution under different working conditions that the film thickness of the cylindrical roller bearing increases gradually with the increase in rotational speed. However, due to the large load present on the roller, the centrifugal force is relatively small, the contact load is less reduced and the oil film pressure does not change significantly.

Figure 6 shows the trend chart of the influence of velocity parameters on film thickness distribution under working conditions 3 and 5. From the necking of the film thickness, it can be seen that as the rotational speed gradually increases, the influence of the thermal effect on the film thickness becomes more obvious, and the central film thickness and the minimum film thickness decrease significantly. The decrease in the oil film thickness

could easily lead to lubrication failure between roller and raceway and could accelerate bearing failure.

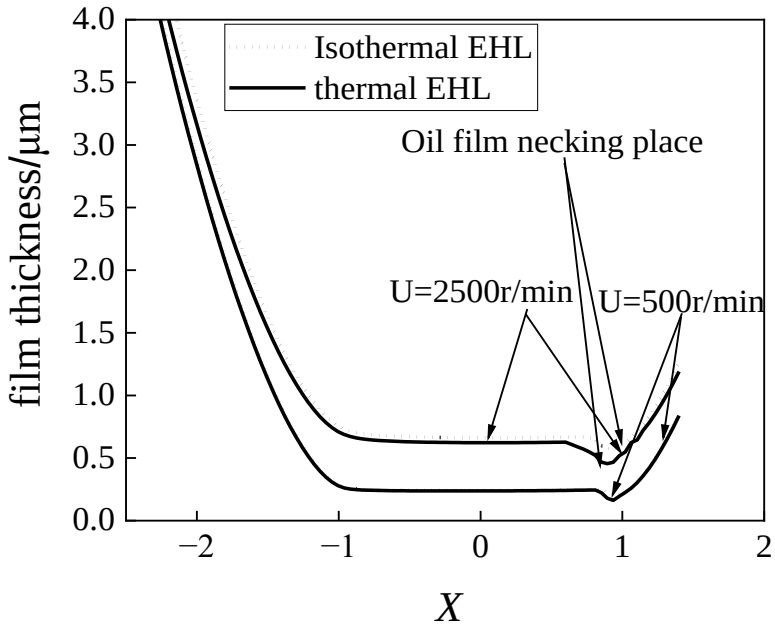


Figure 5. Influence of velocity parameters on thermal EHL.

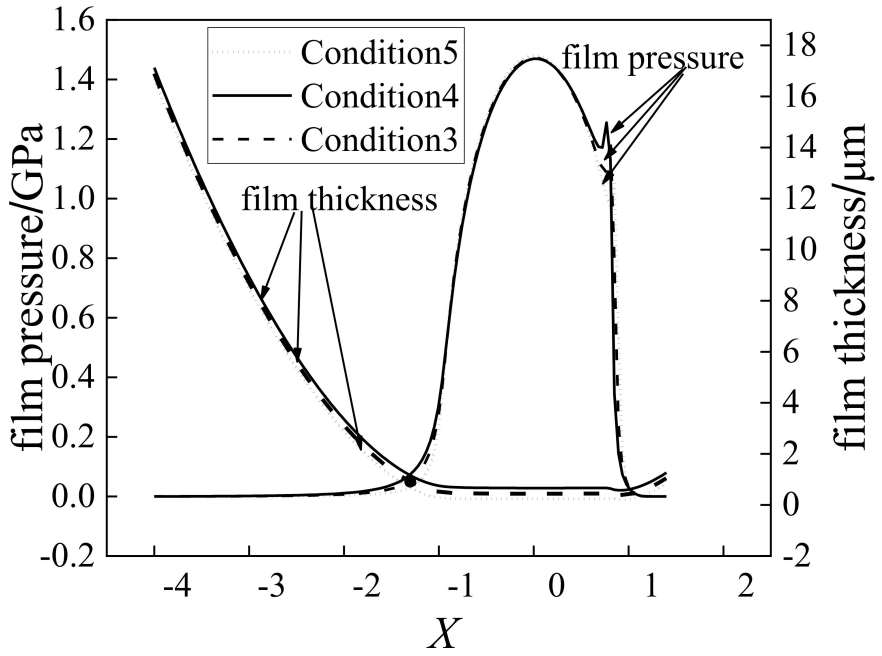


Figure 6. Influence of velocity on film thickness distribution.

Figure 7 shows the trend chart of the influence of speed parameters on oil film pressure under working conditions 3 and 5. From the changing trend of the Isothermal EHL solution and thermal EHL solution shown in Figure 7, it can be seen that the pressure peak of thermal EHL is closer to the inlet region than that of the isothermal solution under consideration of a thermal effect.

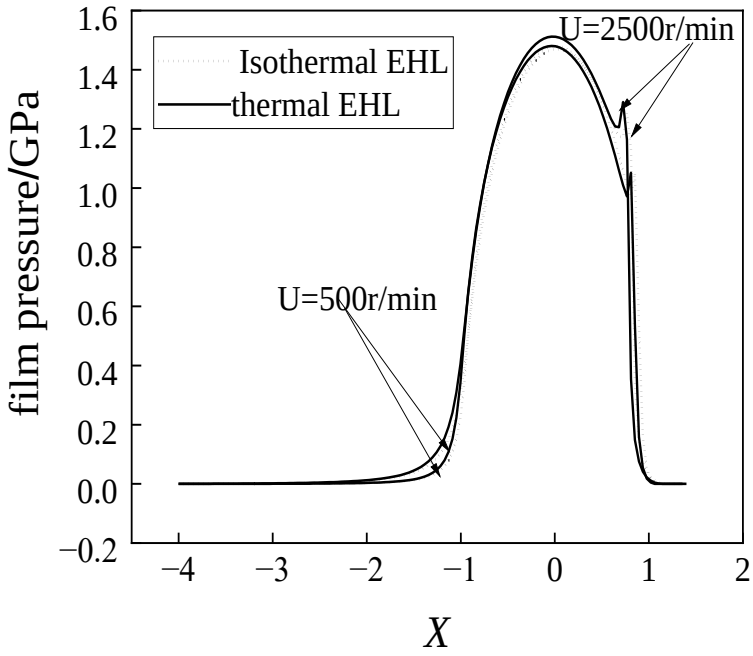


Figure 7. Influence of velocity on oil film pressure distribution.

4.2. Analysis of Bearing Lubrication State

When the roller rolls over the raceway during the bearing operation, the oil layer is rolled to the end, and the appropriate oil amount can give the bearing contact area more film thickness. In this paper, the oil supply conditions of EHL are studied from the perspective of flow balance.

A zero-pressure gradient, two surface contact areas for oil film thickness and effective lubrication film thickness h_{oil} calculation formula is given in [30]:

$$h_{oil} = (\rho_{cen}/\rho_0)h_c \tag{17}$$

In the formula: h_c is the central oil film thickness, ρ_{cen}/ρ_0 reflects the compressibility of the lubricating oil, ρ_{cen} is the lubricating oil density at the center of the contact zone and the value range is 1.01~1.3.

Under the condition of working condition 3, when the inlet position $-X_{in}$ changes from 1.01~4.00, the change trend of effective lubrication film thickness h_{oil} and central film thickness h_c is shown in Figure 8. Figure 8 shows that when $-X_{in}$ is slightly greater than 1, the effective lubrication film thickness and central film thickness increase sharply with the increase in $-X_{in}$, but with the improvement of oil-supply conditions, the change rate decreases gradually, and at $-X_{in} = 2.75$, the effective lubrication film thickness h_{oil} and central film thickness h_c reach the maximum value ($h_{oil} = 0.476\mu$m, $h_c = 0.385$ μm), and gradually stabilize.

Figure 9 shows the oil film pressure and oil film thickness distribution in the $-X_{in} = 1.01$ and $-X_{in} = 2.75$ solutions. Figure 9a shows the oil film pressure close to the Hertz contact pressure under $-X_{in} = 1.01$ conditions. With the increase in $-X_{in}$, the oil film gradually becomes thicker, the outlet necking gradually becomes evident and the second pressure peak of the pressure curve gradually increases.

From Figures 8 and 9, it can be seen that there is a critical value h_{oil} for a given set of operating parameters. The actual h_{oil} is equal to the critical value h_{oil} to achieve the best lubrication effect; when the actual h_{oil} is less than the critical value h_{oil}, the oil film thickness is less than the critical value, and lubrication is insufficient; when the actual h_{oil} is greater than the critical, h_{oil} the excess oil causes heat due to flow, resulting in energy loss, reducing the viscosity of the oil, thereby reducing the lubrication effect.

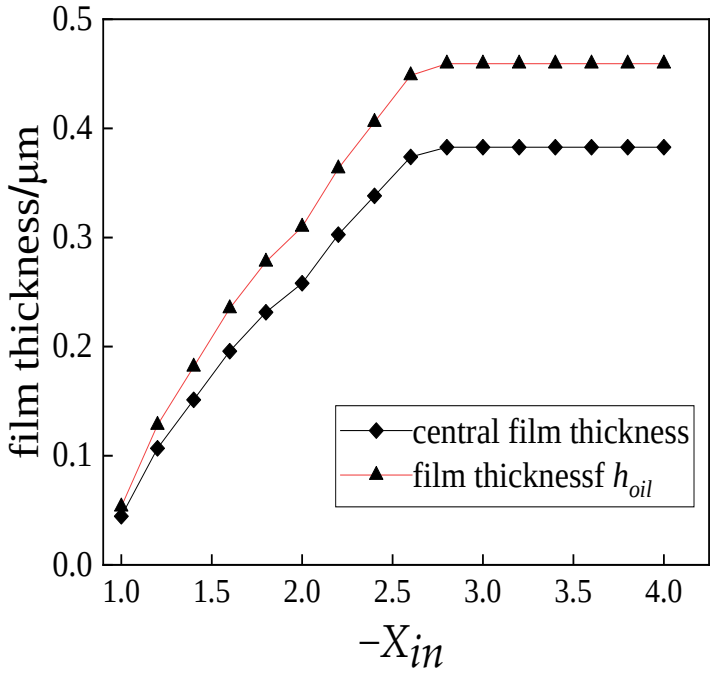


Figure 8. Relationship between film thickness h_{oil} and inlet position $-X_{in}$.

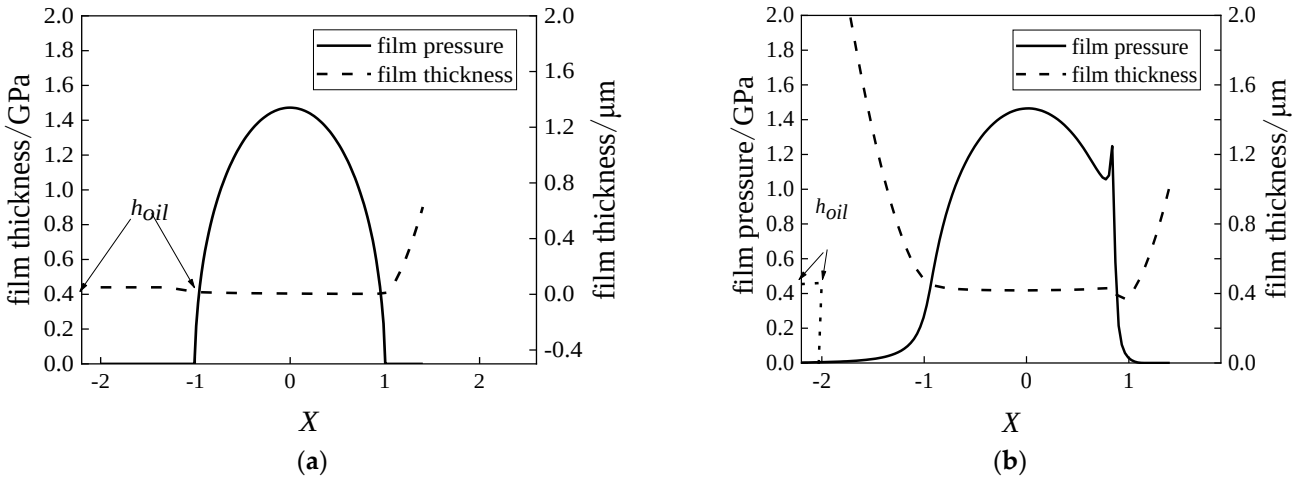


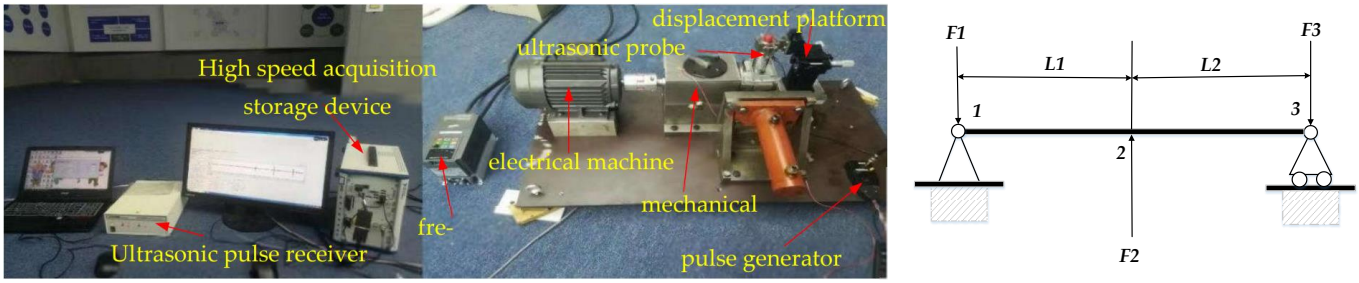
Figure 9. Distribution of oil film pressure and film thickness at different $-X_{in}$ values. (**a**) $-X_{in} = 1.01$; (**b**) $-X_{in} = 2.75$.

5. Experimental Verification

The oil film thickness of the bearing is measured by an ultrasonic measuring instrument, and the numerical calculation results of the theoretical calculation model are verified in this paper. The testing machine includes a driving device, loading device, control device, measurement and data processing system and a lubrication system [31].

Figure 10a shows the bearing film thickness ultrasonic measurement test bench physical diagram, mainly by the bearing test bench, ultrasonic pulse receiver, high-speed acquisition and storage equipment, ultrasonic probe, micro-displacement mobile platform and other components. The function of the micro displacement moving platform is to adjust the position of the probe to facilitate the ultrasonic pulse into the bearing. The test bearing is installed at the right end of the main shaft and is fixed at the bearing seat by the outer shaft. In order to improve the lateral resolution of oil film measurement, and give the sensor a certain adjustment space, we choose the focal length F = 25 mm. The greater the frequency of the ultrasonic wave, the faster the attenuation, so we choose the center

frequency of 50 MHz for the focusing probe. Considering the influence of improving the lateral resolution of film thickness measurement and its installation and debugging, the diameter of the piezoelectric element is selected as 6 mm. According to the frequency requirements, we select the DPR500-300M-RPL2 ultrasonic pulse receiver from JSR. Since the maximum frequency of the ultrasonic pulse is around 100 MHz, NI 's PXIe-5160 acquisition and storage device is selected. Since only the film thickness of the bearing needs to be measured at low speeds, the motor model selected is YE2-80M2-4.



(**a**) Ultrasonic measurement of bearing film thickness test bench physical map. (**b**) Test bearing force diagram

Figure 10. Ultrasonic measurement of bearing film thickness test bench physical map.

Figure 10b is the test-bearing force diagram. In the diagram, 1, 2 and 3 are the porting bearing end, the loading bearing end and the test bearing end, respectively. The radial loading force of the loading system to the spindle is F2, and the direction is vertical. The reaction forces of the spindle-supported bearing and the test bearing are F1 and F3, respectively. It can be seen that the load on the test bearing is:

$$F_3 = \frac{L_1}{L_2 + L_3} F_2 \tag{18}$$

Figure 11 shows a schematic diagram of the principle of ultrasonic measurement of the film thickness of a roller bearing by placing an ultrasonic probe in a tank closely attached to the outer ring of the measured bearing. The ultrasonic probe emits an ultrasonic pulse wave into the water layer, and the ultrasonic wave entering the water layer reaches the water–water tank interface. Some waves are reflected, and some waves are transmitted into the water tank. The ultrasonic wave entering the water channel will eventually partially pass through the outer ring to act on the oil film layer and reflect. The reflected wave is finally detected by the ultrasonic probe after multiple transmissions.

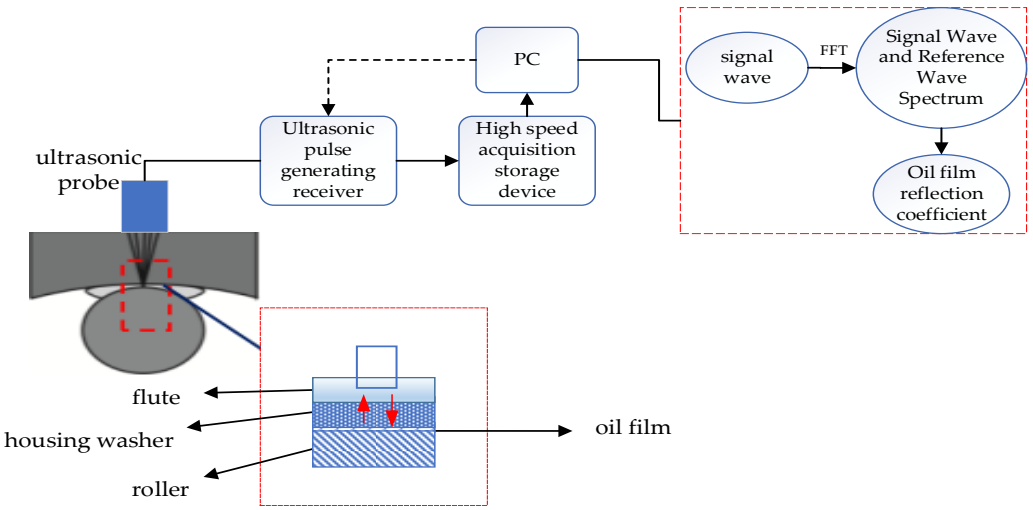


Figure 11. Ultrasonic measurement of roller bearing film thickness principle.

According to the propagation law of ultrasonic waves at the interface, we obtain that there is a relationship between oil film thickness and reflection coefficient. The signal is measured at the same position as the oil film reflection signal, and its reflection coefficient at the oil film position is known. According to the attenuation characteristics of ultrasonic propagation and the propagation law at the interface, it can be approximately considered that the measured sound pressure amplitude ratio of the oil film reflection wave to the reference signal wave is consistent with the sound pressure amplitude ratio of the two at the oil film position. That is:

$$\frac{A_m}{B_m} = \frac{A_I}{B_I} \tag{19}$$

where A_m is the amplitude of the oil film reflection wave signal received by the ultrasonic probe; B_m represents the amplitude of the reference signal received by the ultrasonic probe; A_I represents the amplitude of the reflected wave signal of the oil film layer at the interface between the oil film and the outer ring; B_I represents the reference signal amplitude of the oil film and outer ring interface.

It is assumed that A_f represents the amplitude of the reference signal received by the ultrasonic probe, and A_o represents the amplitude of the reflected wave signal received by the ultrasonic probe. R_f represents the reflection coefficient of the reference signal at the interface of the outer ring raceway, and R_o represents the reflection coefficient of the oil film layer. The reflection coefficient of the oil film layer of the measured signal can be determined by the following formula:

$$R_o = \frac{A_f}{A_o} R_f \tag{20}$$

The peak value of the reflected echo signal is extracted, and the reflectivity of the contact interface is obtained by combining the reference signal of the steel–oil interface. The measured oil film thickness H is calculated. The calculation formula is:

$$H = \frac{2\rho_0 c_0}{wz} \sqrt{\frac{R^2}{1 - R^2}} \tag{21}$$

where ρ_0 is the density of lubricating oil, c_0 is the sound velocity in lubricating oil, ρ is the density of bearing steel, c is the sound velocity in bearing steel, z is the acoustic impedance of bearing steel, $z = \rho c$ and R are the reflection coefficient of ultrasonic signal.

The oil film reflection coefficient is obtained via fast Fourier analysis of the obtained oil film reflection wave and the reference signal wave. According to the relationship between reflection coefficient and oil film thickness, the average oil film thickness in the ultrasonic pulse region is obtained.

Based on the above steps, the test bearing should be cleaned before the experiment so that there is no lubricating oil on the outer ring raceway. First, kerosene is used for cleaning, and then alcohol is used for cleaning. During alcohol cleaning, the residual lubricating oil in the bearing raceway is cleaned with an ultrasonic cleaner. The cleaned bearing is mounted on the bearing seat, and the load is 12 kg, then the ultrasonic probe is adjusted to the appropriate position, with the outer ring raceway of the reflected wave as a reference wave. Based on the working conditions, 4109 lubricating oil is selected, and then injected into the bearing seat through the oil injection hole. The film thickness measurement experiment is carried out at speeds of 300, 350, 400, 450, 500 r/min.

Figure 12 is the minimum film thickness value calculated theoretically under different working conditions. From Figure 12a, it can be seen that the film thickness decreases with the increase in load, and from Figure 12b, it can be seen that the film thickness increases with the increase in speed.

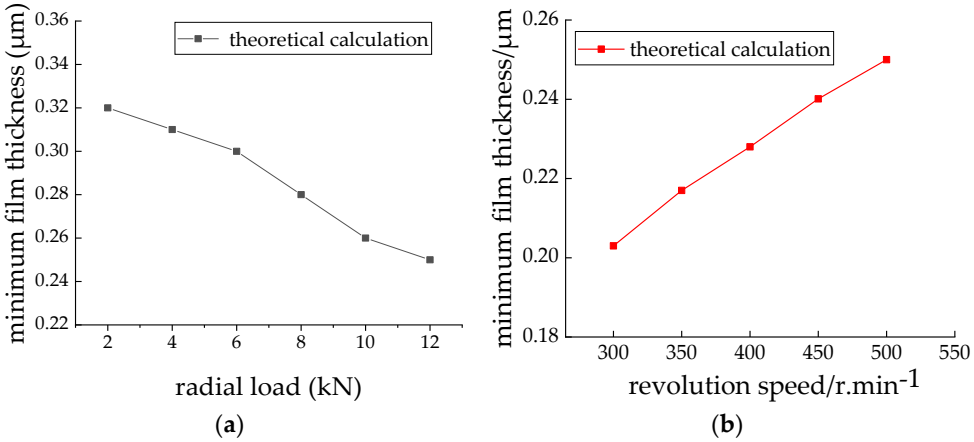


Figure 12. Theoretical minimum film thickness under different conditions. (**a**) radial load; (**b**) revolution speed.

A total of five measurements were taken, and the average film thickness was taken as the final measured value. Table 4 shows the comparison of the measured and theoretical results at different speeds. From the table, it can be seen that with the increase in rotational speed, the oil film thickness shows a gradual increase trend. This is the same trend as the theoretical calculation, and the error is within 10%, in line with the allowable range of error. The measurement result is greater than the theoretical prediction value, mainly because the result of ultrasonic reflection method is the average film thickness of the focused area of the ultrasonic probe, and the theoretical calculation result provides the minimum film thickness.

Table 4. Comparison of experimental measurement and theoretical calculation results at different speeds.

Theoretical Calculation of Film Thickness/μm Measurement Serial Number	First /μm	Second /μm	Third /μm	Fourth /μm	Fifth /μm	Mean Value /μm	Error
0.197	0.218	0.213	0.217	0.214	0.209	0.2142	8.0%
0.213	0.231	0.230	0.232	0.235	0.228	0.2312	7.8%
0.228	0.253	0.252	0.247	0.250	0.249	0.2502	8.8%
0.241	0.263	0.259	0.262	0.256	0.258	0.2596	7.1%
0.252	0.272	0.269	0.271	0.268	0.275	0.2710	7.0%

We repeat the above steps, fix the speed at 500 r/min, inject lubricating oil and adjust the load from 2000 to 12,000 N. The comparison between theoretical calculation and measurement results under different loads is shown in Table 5. It can be seen from Table 5 that as the load increases, the film thickness gradually becomes smaller, and the trend is the same, and the error is within the allowable range. The measurement results are larger than the theoretical results, which is also due to the average effect of the ultrasonic probe.

Table 5. Comparison of experimental measurement and theoretical calculation results under different load conditions.

Theoretical Calculation of Film Thickness/μm Measurement Serial Number	First /μm	Second /μm	Third /μm	Fourth /μm	Fifth /μm	Mean Value /μm	Error
0.32	0.341	0.338	0.337	0.340	0.336	0.3384	5.4%
0.31	0.331	0.329	0.330	0.327	0.334	0.3302	6.1%
0.30	0.323	0.319	0.321	0.320	0.324	0.3214	6.6%
0.28	0.301	0.304	0.313	0.321	0.297	0.3072	8.8%
0.26	0.286	0.279	0.281	0.285	0.281	0.2824	8.4%
0.25	0.266	0.271	0.275	0.273	0.268	0.2706	7.6%

6. Conclusions

In this paper, based on the ultrasonic measurement test bench of oil film thickness of cylindrical roller bearing, combined with theoretical analysis and experiments, the influence of thermal effect on the lubrication performance of cylindrical roller bearing under different speeds and loads is studied. The following conclusions are obtained:

(1) With the increase in rotational speed, the film thickness of cylindrical roller bearing increases gradually, but the oil film pressure does not change significantly. The thermal effect on the film thickness is more and more obvious; the center film thickness and minimum film thickness decrease significantly. Considering the thermal effect, the pressure peak of the thermoelastic flow is closer to the inlet region than the isothermal flow.

(2) As the radial load increases, the maximum oil film pressure gradually increases. The film thickness gradient in the inlet area is greatly reduced, and the center film thickness is almost unchanged. The thermal effect does not influence the film thickness as a whole, but the minimum oil film thickness gradually decreases.

(3) For a given working condition, there is a critical value of effective lubrication film thickness. When the actual lubrication film thickness is equal to the critical value, the best lubrication state of the bearing is reached.

(4) We have provided an accurate and efficient solution for the study of bearing lubrication characteristics under harsh conditions, and a theoretical basis for revealing the bearing lubrication mechanism. It prolongs the life of the bearing, reduces the company's economic losses and improves the safety of the industry, providing protection for the safety of operators;

(5) Because the bearing oil film thickness is thin and difficult to measure, the existing methods still lead to errors when it comes to measuring the film thickness distribution. This lays a foundation for further study of multi-body elastohydrodynamic lubrication characteristics in the future, and also opens up the study of the interaction between the oil film thickness when the rolling element is lubricated with the inner and outer rings at the same position.

Author Contributions: Conceptualization, M.Z.; methodology, M.Z. and N.G.; software, M.Z.; validation, X.M. and M.Z.; investigation, Y.X.; resources, X.M.; data curation, N.G.; writing—original draft preparation, M.Z.; writing—review and editing, J.L.; supervision, Y.X.; project administration, X.M.; funding acquisition, X.M. All authors have read and agreed to the published version of the manuscript.

Funding: This research was funded by National Key R & D Program of China (Grant No. 2021YFB2011000); Henan Science and Technology Project (212102210365) and Research Program in University of Henan Province (Grant No. 21A460014).

Institutional Review Board Statement: Not applicable.

Informed Consent Statement: Not applicable.

Data Availability Statement: Data are contained within the article.

Conflicts of Interest: The authors declare no conflict of interest.

References

1. Konopka, D.; Pape, F.; Heimes, N. Functionality Investigations of Dry-Lubricated Molybdenum Trioxide Cylindrical Roller Thrust Bearings. *Coatings* **2022**, *12*, 591. [CrossRef]
2. Xie, X.; Xu, J.; Luo, J. Analysis of skid damage to cylindrical roller bearing of mainshaft of aeroengine. *J. Mech. Sci. Technol.* **2020**, *34*, 3239–3247. [CrossRef]
3. Hao, X.; Gu, X.; Zhou, X. Distribution characteristics of stress and displacement of rings of cylindrical roller bearing. *J. Mech. Eng. Sci.* **2019**, *233*, 4348–4358. [CrossRef]
4. Cao, H.; Su, S.; Jing, X. Vibration mechanism analysis for cylindrical roller bearings with single/multi defects and compound faults. *Mech. Syst. Signal Process.* **2020**, *144*, 106903. [CrossRef]

5. Liu, Y.; Zhang, Z. Skidding research of a high-speed cylindrical roller bearing with beveled cage pockets. *Ind. Lubr. Tribol.* **2020**, *72*, 969–976. [CrossRef]
6. Sun, X.; Zhang, W.; Tian, H. Theoretical analysis of cylindrical roller bearing with flexible rings mounted in groove elastic support. *J. Adv. Mech. Des. Syst. Manuf.* **2020**, *14*, JAMDSM0102. [CrossRef]
7. Guo, Y.; Keller, J. Validation of combined analytical methods to predict slip in cylindrical roller bearings. *Tribol. Int.* **2020**, *148*, 106347. [CrossRef]
8. Tsuha, N.A.H.; Cavalca, K.L. Stiffness and damping of elastohydrodynamic line contact applied to cylindrical roller bearing dynamic model. *J. Sound Vib.* **2020**, *481*, 115444. [CrossRef]
9. Niu, L.; Cao, H.; Hou, H. Experimental observations and dynamic modeling of vibration characteristics of a cylindrical roller bearing with roller defects. *Mech. Syst. Signal Process.* **2020**, *138*, 106553. [CrossRef]
10. Qiu, L.; Liu, S.; Chen, X. Lubrication and loading characteristics of cylindrical roller bearings with misalignment and roller modifications. *Tribol. Int.* **2022**, *165*, 107291. [CrossRef]
11. Liu, X.; Xin, Z.; Zhou, J. Analysis of thermal dynamic micro-EHL considering bearing assembly temperature. *J. Eng. Tribol.* **2021**, *235*, 1283–1297. [CrossRef]
12. Tang, H.; Wang, J.; Sun, N. Effect of angular speed of cam on oil film variation in the line contact thermal EHL of a cam-tappet pair. *Ind. Lubr. Tribol.* **2020**, *72*, 713–722. [CrossRef]
13. Hultqvist, T.; Vrček, A.; Marklund, P. On waviness and two-sided surface features in thermal elastohydrodynamically lubricated line contacts. *Lubricants* **2020**, *8*, 64. [CrossRef]
14. Marian, M.; Bartz, M.; Wartzack, S. Non-dimensional groups, film thickness equations and correction factors for elastohydrodynamic lubrication. *Lubricants* **2020**, *8*, 95. [CrossRef]
15. Liu, S.; Qiu, L.; Chen, X. In-Depth Exploration of the Multigrid Method to Simulate Elastohydrodynamic Line Lubrications With Smooth, Wavy, and Rough Surfaces. *J. Tribol.* **2021**, *143*, 121602. [CrossRef]
16. Zhao, Y.; Wong, P.L. Thermal-EHL analysis of slip/no-slip contact at high slide-to-roll ratio. *Tribol. Int.* **2021**, *153*, 106617. [CrossRef]
17. Yu, Y.; Suh, J. Numerical analysis of three-dimensional thermo-elastic rolling contact under steady-state conditions. *Friction* **2022**, *10*, 630–644. [CrossRef]
18. Bai, X.; Dong, Q.; Zheng, H.; Zhou, K. A Finite Element Model for Non-Newtonian Starved Thermal-Elastohydrodynamic Lubrication of 3D Line Contact. *Int. J. Appl. Mech.* **2021**, *13*, 2150107. [CrossRef]
19. Duan, Z.; Wu, T. Lubrication state identification of the line contact tribo-pair under a pure rolling condition with ultrasonic method. *J. Eng. Tribol.* **2022**, *236*, 982–994. [CrossRef]
20. Li, M.; Tian, G.; Liu, Y. Utrasollic measurement of on film thickness in cylindrical roller bearings under mixed lubrication. *Vibr. Shock* **2020**, *39*, 279–284.
21. Beamish, S.; Reddyhoff, T.; Hunter, A. A method to determine acoustic properties of solids and its application to measuring oil film thickness in bearing shells of unknown composition. *Measurement* **2022**, *195*, 111176. [CrossRef]
22. Liu, M.; Ku, H.; Zhang, J. Predicting fatigue life for finite line contact under starved elastohydrodynamic lubrication condition. *Math. Probl. Eng.* **2020**, *2020*, 5928621. [CrossRef]
23. Lin, W.; Li, J.; Zhang, Y. Comparison of the Models for Multiscale Elastohydrodynamic Lubrication in a Line Contact. *J. Appl. Fluid Mech.* **2022**, *15*, 515–521.
24. Li, J.; Zhang, Y. Multiscale Hydrodynamics in Line Contacts with Different Fluid-Contact Interactions. *J. Appl. Fluid Mech.* **2021**, *14*, 1767–1773.
25. Duan, H.; Song, J.; Wang, Z. Lubrication and Fatigue Life Evaluation of High-Speed Cylindrical Roller Bearing under Misalignment. *Math. Probl. Eng.* **2020**, *2020*, 2068924. [CrossRef]
26. Hao, X.; Yun, X.; Han, Q. Thermal-fluid-solid coupling in thermal characteristics analysis of rolling bearing system under oil lubrication. *J. Tribol.* **2020**, *142*, 031201. [CrossRef]
27. Chippa, S.P.; Borse, N.V. Transient elastohydrodynamic analysis of finite line contact under load impulse. *J. Eng. Tribol.* **2021**, *235*, 1526–1540. [CrossRef]
28. Zhang, C.; Guo, D.; Tian, J. Research on the influencing factors of thermal characteristics of high-speed grease lubricated angular contact ball bearing. *Adv. Mech. Eng.* **2021**, *13*. [CrossRef]
29. Liqin, W.; Yufan, L. Geometric modification on mixed lubrication performance of low-speed cylindrical roller bearing. *Tribology* **2019**, *39*, 470–478.
30. Yang, P.; Cui, J.; Jian Tian, Z. Analysis of oil supply conditions for linear contact elastohydrodynamic lubrication. *J. Tribol.* **2006**, *26*, 242–246.
31. Nicholas, G.; Clarke, B.P.; Dwyer-Joyce, R.S. Detection of lubrication state in a field operational wind turbine gearbox bearing using ultrasonic reflectometry. *Lubricants* **2021**, *9*, 6. [CrossRef]

Disclaimer/Publisher's Note: The statements, opinions and data contained in all publications are solely those of the individual author(s) and contributor(s) and not of MDPI and/or the editor(s). MDPI and/or the editor(s) disclaim responsibility for any injury to people or property resulting from any ideas, methods, instructions or products referred to in the content.